Biophysical Journal, Volume *111*

Supplemental Information

Glycoprotein Ib-IX-V Complex Transmits Cytoskeletal Forces That Enhance Platelet Adhesion

Shirin Feghhi, Adam D. Munday, Wes W. Tooley, Shreya Rajsekar, Adriane M. Fura, John D. Kulman, Jose A. López, and Nathan J. Sniadecki

Supporting Information

SI Materials and Methods

Fabrication of the Nanopost Array Silicon Master. A silicon wafer was spin-coated with a 1.55 μm-thick layer of ma-N 2410 resist (Micro Resist Technology, GmbH, Berlin, Germany). The resist was patterned with circles that were 850 nm in diameter and 2 μm in center-to-center spacing using a JEOL JBX-6300FS e-beam lithography system (100 kV energy, 20 nA current). The resist was developed in MF-319 developer (Shipley Company, Marlborough, MA), and then etched with a fluorine-based inductively coupled plasma (ICP) process using an Oxford PlasmaLab 100 system to create a silicon master with an array of vertical cantilevers. Using scanning electron microscopy (SEM), we measured the dimensions of the silicon nanoposts in the array to be 850 nm in diameter, 2 μm in spacing, and 3.5 μm in height (Fig. S1 *A*).

Soft Lithography. A double-casting technique was used to replicate the features of the silicon master in polydimethylsiloxane (PDMS) (Sylgard 184, Dow Corning, Midland, MI). Following a process that has been previously described for microposts (19), we made a negative mold by casting a 10:1 ratio of base-to-curing agent of PDMS from the silicon master and then passivating its surface with (tridecafluoro-1,1,2,2-tetrahyrooctyl)-1-trichlorosilane (United Chemical Technologies, Bristol, PA). We poured liquid PDMS into the negative molds, placed a clean glass slide on top of the liquid PDMS, and baked it at 110 $^{\circ}$C for 15 hours. Once the PDMS was cured and permanently bonded to

the glass, we peeled it from the negative mold to create an array of PDMS nanoposts that were freestanding. We repeated the double-casting process to make new arrays of nanoposts for each experiment.

We noted that PDMS nanoposts did not replicate the exact dimensions of the original silicon master (Fig. S1 *B*). Using SEM, we measured the dimensions of the PDMS nanoposts to be 850 nm in diameter (*d*), 2 μm in spacing, and 2.5 μm in height (*L*). These dimensions were consistent between nanopost arrays that were replicated from the same master. For PDMS baked at 110 $^{\circ}$C for 15 hours, we measured the Young's modulus of PDMS (*E*) to be 3.2 MPa using tensile testing. In accordance with Euler-Bernoulli beam theory, the bending stiffness of the arrays was calculated to be $k = 3\pi Ed^4/64L^3$ = 15.7 nN/μm (Fig. S3).

Scanning Electron Microscopy. Samples of platelets on nanoposts were dried using critical point drying techniques, as described previously (35). In brief, we dehydrated the samples by incubation in dishes of 50%, 70%, 80%, 90%, and 100% ethanol for 10 minutes each. A critical point drying system (CPD) (Polaron E3100; Quorum, Houston, TX) was then used to dry the samples overnight to prevent damage to the platelets and nanoposts. Dried samples were given a conductive coating by sputtering with gold-palladium (60%-to-40%) for 90 seconds. The samples were imaged using a scanning electron microscope (SEM) (FEI Sirion) with a voltage of 5 kV at a working distance of 10 mm. As others have noted, drying biological samples with CPD causes their structures to shrink (36). We observed shrinkage in our samples of platelets on

nanoposts from CPD because the deflections of the nanoposts were substantially larger than the deflections observed using confocal microscopy.

Confocal Microscopy. To acquire images of the platelets and nanoposts, we used a confocal microscope (Zeiss LSM 510) equipped with a 63× oil objective (NA 1.42). A step size of 0.31 μm was used to construct a Z-stack of platelets and nanoposts (Fig. 1 *B-C*). We then extracted the raw images for image analysis of the nanoposts and platelets.

Force and Spread Area Analysis. A manual code was developed in MATLAB to analyze the images of the samples obtained from confocal microscopy. The deflections of the nanoposts were determined by comparing the centroids of the nanoposts in the confocal images taken at the top and base of the nanoposts. We calculated the force vector at each nanopost by multiplying the measured deflections by the bending stiffness of the nanoposts. We calculated the total force per platelet by the sum of the magnitudes of the force vectors at each nanopost underneath a platelet. Spread area was quantified from the actin image using the outer edge of the cell on the posts.

Fabrication of Micropost Array SU-8 Master. The process of fabricating arrays of microposts has been previously described (1). In brief, a silicon wafer was spin-coated with a 5-μm layer of SU-8 2005 (MicroChem Corp., Newton, MA). The base layer of resist was flood-exposed with UV light to cross-link the SU-8. The wafer was spin-

coated with a 7-μm layer of SU-8 2010. A chrome mask containing the features of the microposts was used to selectively expose the second layer of SU-8 with UV light. The unexposed regions in the SU-8 layer were removed using SU-8 developer (MicroChem Corp.) to make arrays of microposts that were 2.39 μm in diameter, 6 μm in spacing, and 6.98 μm in height. This array was used for all the experiments done with CHO cells except for the blebbistatin force-inhibition assays. We used the same protocol to make a second array of microposts that were 1.75 μm in diameter, 6 μm in spacing, and 4.14 μm in height. These arrays were used for the blebbistatin force-inhibition assays as described above.

To make PDMS replicates of the microposts, we used a double casting process that was similar to the process for PDMS nanoposts, but with the exception that the arrays of PDMS microposts were baked for 6 hours at 110 $^{\circ}$C, yielding a Young's modulus of 3.1 MPa for PDMS. Therefore, the bending stiffness of the micropost arrays was calculated to be 43.6 nN/μm for the first array and 54.9 nN/μm for the second array.

Fluorescent Microscopy. We captured fluorescent z-stacks of CHO cells on microposts using an Olympus IX-81 microscope with a spinning disc confocal and a 40× oil objective (NA 1.3). The forces and spread area were calculated with a MATLAB 7.1 code that processed the images in a manner similar to the code used to analyze platelets on nanoposts. We measured the force vector at each micropost under a CHO cell and reported the average magnitude as the force per post.

Constructing pBIG-4e and pBIG-4f. The cDNA encoding green fluorescent protein (GFP) was excised from plasmid pEGFP-N1 (Clontech Laboratories, Mountain View, CA; Genbank accession no. U55762) by digestion with *Sal*I and *Not*I restriction endonucleases and ligated into the corresponding restriction sites of plasmid pIRES (Clontech Laboratories) to generate vector pBIG-St1. The IRES-GFP cassette was excised from pBIG-St1 by digestion with *Not*I, blunt-end fill-in with T4 DNA polymerase, and subsequent digestion with *Nhe*I. The resulting fragment was ligated into pBI (Clontech Laboratories; Genbank accession no. U89932), which had been digested with *Nhe*I and *Eco*RV. The resulting vector was designated pBIG-St2. The DNA sequence encompassing the Kozak sequence, start codon and the coding sequence of the bovine prolactin signal peptide and BirA (*E. coli* biotin ligase) were both amplified by PCR from plasmid pCBioSec (37) and ligated into plasmid pBIG-St2 that had been digested with *Pst*I and *Not*I. The resulting vector was designated pBIG-St3. Finally, the Kozak sequence, start codon, α1-antitrypsin signal peptide coding sequence, multiple cloning site (MCS) and biotin acceptor peptide (BioTag) (38) coding sequence of plasmid pCBioSec were PCR amplified and ligated into plasmid pBIG-St3 that had been

digested with *Nhe*I and *Nsi*I. The resulting vector was designated pBIG-4e. Plasmid pBIG-4f was constructed in a similar manner, except that a DNA sequence encoding an epitope tag for antibody HPC4 (39) was inserted 5' to the BioTag sequence.

Additional References

35. Barrett, L. A., and R. E. Pendergrass. 1977. Method for Handling Free Cells through Critical-Point Drying. Journal of Microscopy-Oxford 109:311-313.

36. Gusnard, D., and R. H. Kirschner. 1977. Cell and organelle shrinkage during preparation for scanning electron microscopy: effects of fixation, dehydration and critical point drying. J Microsc 110:51-57.

37. Kulman, J. D., M. Satake, and J. E. Harris. 2007. A versatile system for site-specific enzymatic biotinylation and regulated expression of proteins in cultured mammalian cells. Protein Expr Purif 52:320-328.

38. Schatz, P. J. 1993. Use of peptide libraries to map the substrate specificity of a peptide-modifying enzyme: a 13 residue consensus peptide specifies biotinylation in Escherichia coli. Biotechnology (N Y) 11:1138-1143.

39. Stearns, D. J., S. Kurosawa, P. J. Sims, N. L. Esmon, and C. T. Esmon. 1988. The interaction of a Ca2+-dependent monoclonal antibody with the protein C activation peptide region. Evidence for obligatory Ca2+ binding to both antigen and antibody. J Biol Chem 263:826-832.

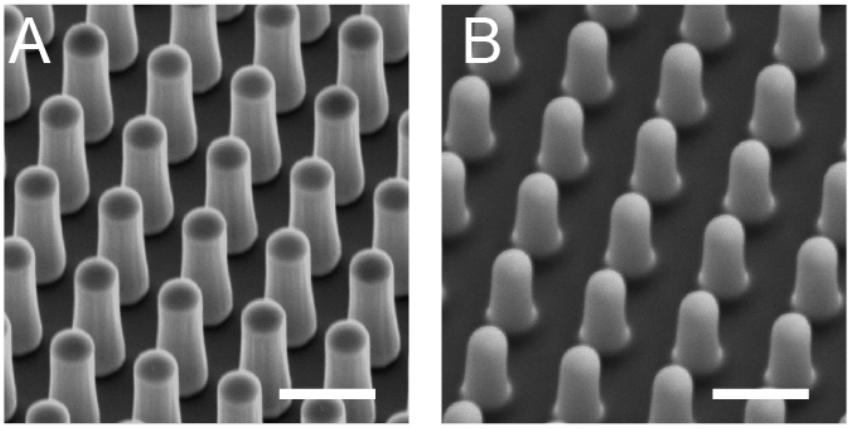

Figure S1 – SEM micrograph of, *(A)* an array of silicon nanoposts and, *(B)* a PDMS replicate of the array. Scale bars are 2 µm.

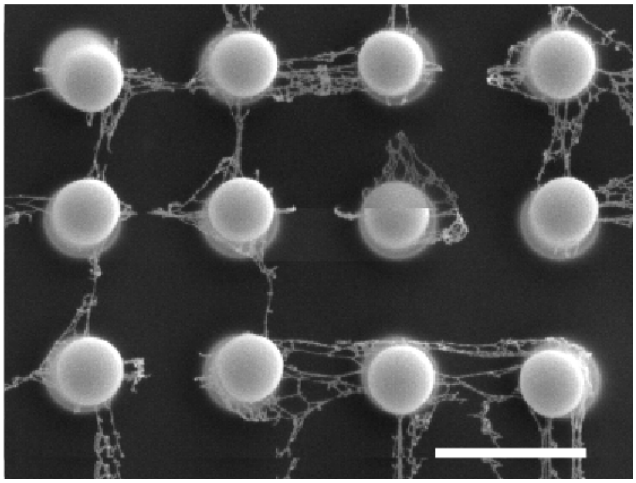

Figure S2 – SEM micrograph of VWF strands that formed on the tips of the PDMS nanoposts. Scale bar is 2 μm.

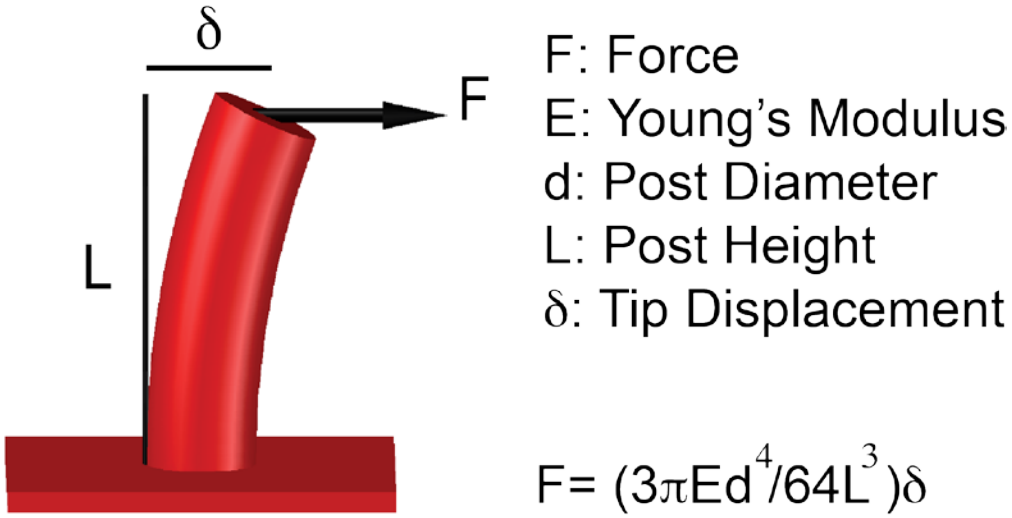

Figure S3 – The calculation of force on a nanopost by a platelet is based on the Young's modulus of PDMS (E) and the length (L), diameter (d), and deflection (δ) of the nanopost.

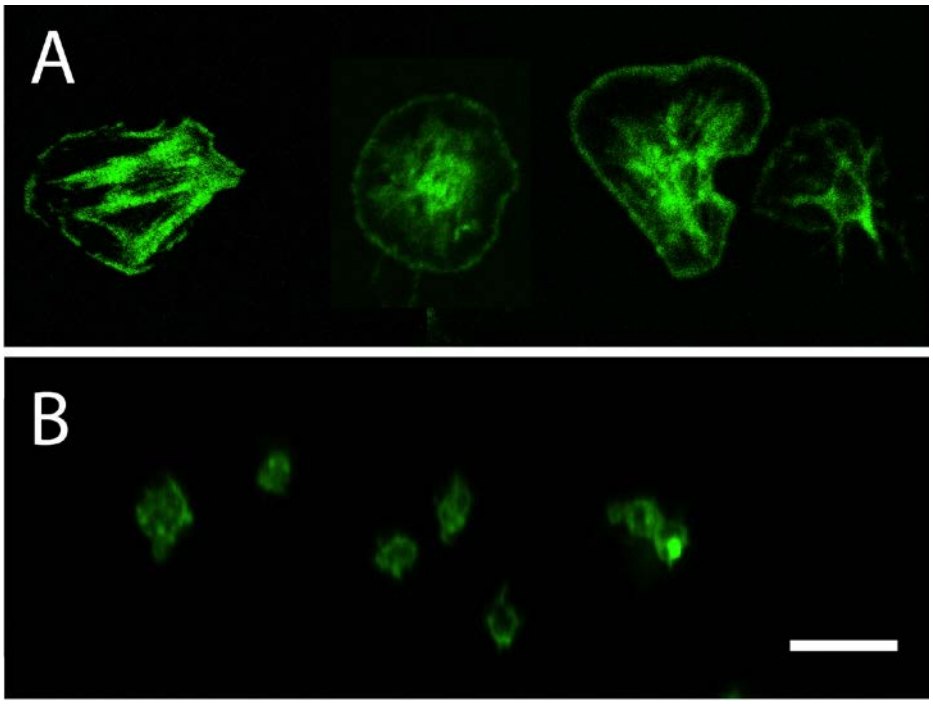

Figure S4 – Micrographs from confocal microscopy of platelets adhered onto flat surfaces of PDMS that were coated with *(A)* VWF or *(B)* recombinant A1 domain. Platelet morphologies on VWF or A1 domain as depicted by phalloidin staining are similar to that of platelets on nanoposts coated with VWF or A1 domain, respectively, as shown in Fig. 2 *A* and Fig. 3 *C*. Scale bar is 5 μm.

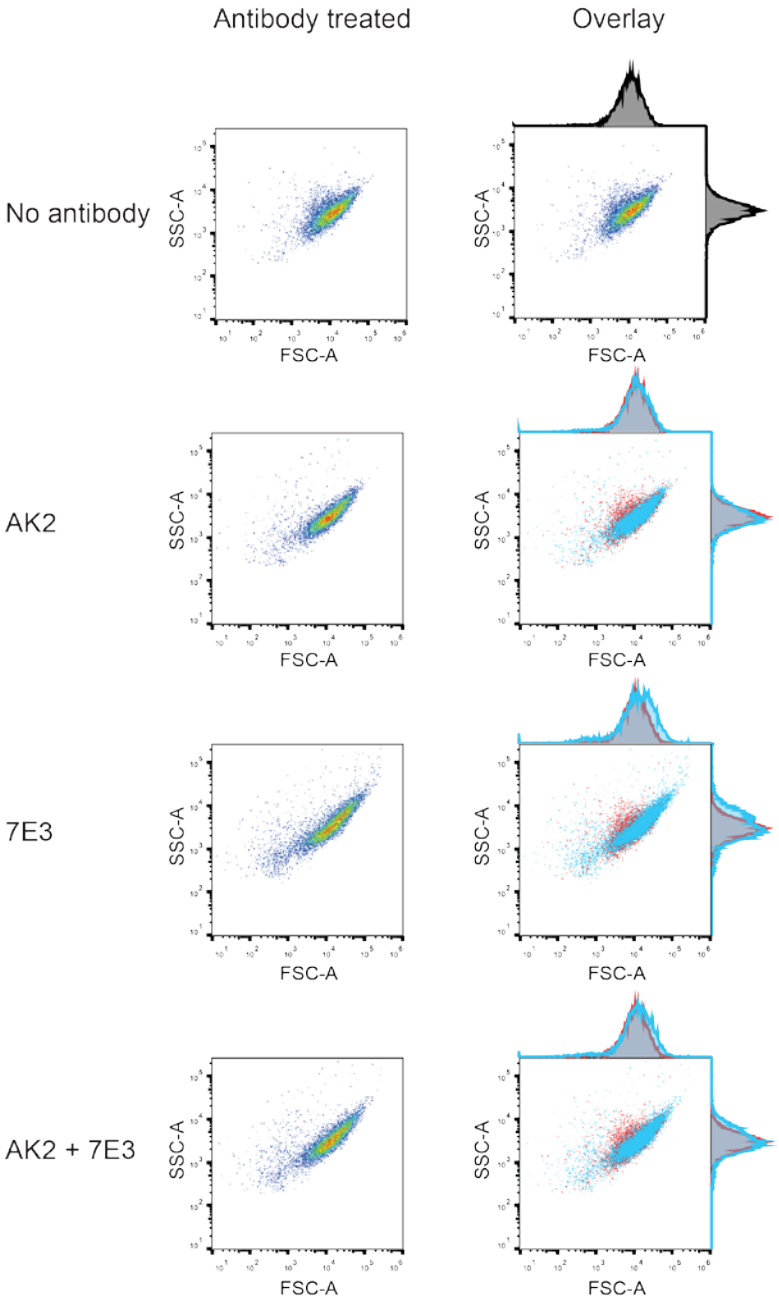

Figure S5 – Dot plots and histograms of platelets indicating that platelets were not activated by antibody treatment.

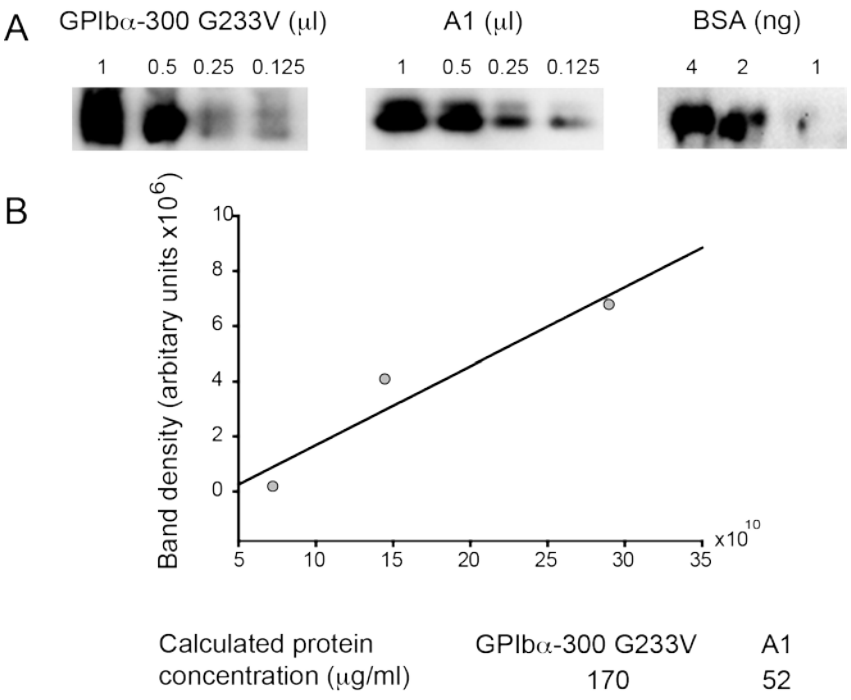

Figure S6 – *(A)* Representative immunoblots of GPIbα-300 G233V (Ibα300gof), A1 domain, and biotin-BSA. *(B)* Calculated protein concentration using the standard curve for Ibα300gof and A1 domain.

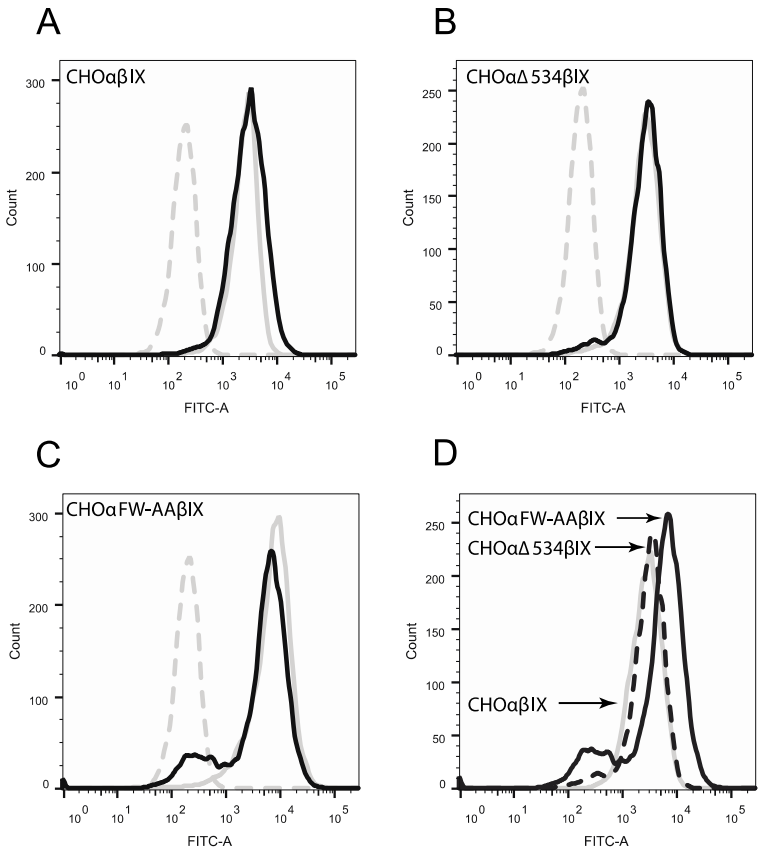

Figure S7 – Flow cytometry histogram of cell surface expression of GPIbα and GPIX in *(A)* CHOαβIX cells, and *(B)* CHOαΔ534βIX cells *(C)* CHOαFW-AAβIX cells. Grey dotted line denotes IgG, solid grey line denotes GPIX, and solid black line denotes GPIbα. *(D)* Overlay of flow cytometry histograms of GPIbα surface expression from CHOαβIX (dashed line) and CHOαΔ534βIX (solid line) shows that surface expression is similar for the two CHOαΔ534βIX and CHOαβIX cell lines and slightly higher for CHOαFW-AAβIX cells.

Table S1. Force and Area per Donor in Fig. 2

	Force (nN)				Area (μm^2)			
Subject	*Control*	*AK2*	*7E3*	*AK2+7E3*	*Control*	*AK2*	*7E3*	*AK2+7E3*
Donor 1	53.2±40.2 (20)	45.8±37.4 (27)	19.7±23.5 (29)	4.6±1.7 (35)	28.0±16.4 (20)	21.4±13.3 (27)	12.3±8.5 (29)	5.4±1.4 (35)
Donor 2	100.3±33.3 (7)	80.7±35.0 (14)	46.3±28.5 (7)	*	40.8±18.2 (7)	25.8±12.4 (14)	27.6±13.7 (7)	*
Donor 3	26.1±18.5 (20)	25.4±16.8 (24)	16.7±20.1 (20)	13.5±13.1 (15)	24.3±14.9 (20)	25.0±15.4 (24)	14.4±12.1 (20)	15.6±11.6 (15)
Donor 4	33.3±26.5 (18)	26.9±29.0 (11)	26.2±32.4 (8)	8.5±10.8 (4)	28.8±21.2 (18)	21.1±17.9 (11)	17.3±16.2 (8)	13.0±8.5 (4)
Donor 5	76.0±41.3 (12)	46.1±39.7 (27)	12.5±18.2 (18)	16.4±25.8 (20)	38.0±19.0 (12)	21.0±19.4 (27)	8.0±5.5 (18)	8.8±9.4 (20)

Results per donor for these studies are shown as mean ± standard deviation. The number of platelets analyzed per condition is shown in parentheses. The normalized results are shown in Fig. 2. Asterisk (*) indicates that platelets did not adhere to the array.

Table S2. Force and Area per Donor in Fig. 3

	Force (nN)			Area (μm^2)		
Subject	*Control*	*Ibα300gof*	*A1 domain*	*Control*	*Ibα300gof*	*A1 domain*
Donor 1	42.9±29.1 (33)	38.8±29.4 (24)	10.8±7.8 (29)	25.7±16.5 (33)	21.3±15.4 (24)	9.0±7.1 (29)
Donor 2	86.8±64.1 (19)	38.0±39.1 (30)	16.3±13.7 (36)	37.4±28.7 (19)	25.7±22.1 (30)	11.3±6.8 (36)
Donor 3	47.2±26.4 (32)	14.5±15.8 (33)	2.5±0.8 (36)	24.1±14.8 (32)	12.7±8.9 (33)	4.9±1.8 (36)
Donor 4	45.2±20.0 (22)	43.1±20.4 (24)	10.3±5.8 (25)	25.0±12.4 (22)	17.2±10.4 (24)	8.0±3.2 (25)
Donor 5	47.4±27.0 (24)	41.9±23.5 (30)	1.8±0.6 (18)	20.7±12.4 (24)	16.5±8.6 (30)	3.5±2.1 (18)

Results per donor for these studies are shown as mean ± standard deviation. The number of platelets analyzed per condition is shown in parentheses. The normalized results are shown in Fig. 3.

Table S3. Platelet Count per Field

Subject	Control	Blebbistatin
Donor 1	12±5.7 (10)	7.8±8.5 (10)
Donor 2	8.7±8.5 (10)	1.3±0.8 (10)
Donor 3	4.9±9.1 (9)	1.5±2.8 (10)
Donor 4	1.9±1.1 (10)	1.3±0.9 (10)

Results per donor for these studies are shown as mean ± standard deviation. The number of platelets analyzed per condition is shown in parentheses. The table shows platelet count per donor for adhesion assay shown in Fig. 5.